

A Unique Modelling Strategy to Dynamically Simulate the Performance of a Lobe Pump for Industrial Applications

Deepak Kumar Kanungo¹, Rabiranjana Murmu², Harekrushna Sutar^{2*}

¹Bharat Heavy Electricals Limited, Corporate R & D, Hyderabad, Telangana, India

²Chemical Engineering Department, Indira Gandhi Institute of Technology, Sarang, Odisha, India

Email: *h.k.sutar@gmail.com

How to cite this paper: Kanungo, D.K., Murmu, R. and Sutar, H. (2024) A Unique Modelling Strategy to Dynamically Simulate the Performance of a Lobe Pump for Industrial Applications. *Advances in Chemical Engineering and Science*, 14, 57-73.
<https://doi.org/10.4236/aces.2024.142004>

Received: March 3, 2024

Accepted: April 7, 2024

Published: April 10, 2024

Copyright © 2024 by author(s) and Scientific Research Publishing Inc.

This work is licensed under the Creative Commons Attribution International License (CC BY 4.0).

<http://creativecommons.org/licenses/by/4.0/>



Open Access

Abstract

The performance of a newly designed tri-lobe industrial lobe pump of high capacity is simulated by using commercial CFD solver Ansys Fluent. A combination of user-defined-functions and meshing strategies is employed to capture the rotation of the lobes. The numerical model is validated by comparing the simulated results with the literature values. The processes of suction, displacement, compression and exhaust are accurately captured in the transient simulation. The fluid pressure value remains in the range of inlet pressure value till the processes of suction and displacement are over. The instantaneous process of compression is accurately captured in the simulation. The movement of a particular working chamber is traced along the gradual degree of lobe's rotation. At five different degrees of lobe's rotation, pressure contour plots are reported which clearly shows the pressure values inside the working chamber. Each pressure value inside the working chamber conforms to the particular process in which the working chamber is operating. Finally, the power requirement at the shaft of rotation is estimated from the simulated values. The estimated value of power requirement is 3.61 BHP + FHP whereas the same calculated theoretically is 3 BHP + FHP. The discrepancy is attributed to the assumption of symmetry of blower along the thickness.

Keywords

CFD, Lobe Pump, Moving Dynamic Mesh, Pressure Fluctuation, Transient Simulation

1. Introduction

Lobe pumps are positive displacement pumps used in many industries such as

oil and gas, mining and chemicals, to transport fluids. These are also used as blowers or vacuum pumps [1]. A typical lobe pump has two rotors rotating in opposite directions. The rotors are attached to two identically shaped lobes. Depending on the number of lobes attached to each rotor, the lobe pump is identified as bi-lobe, tri-lobe, or tetra-lobe lobe pump. With gradual rotation of lobes, certain amount of fluid gets trapped in between the lobes and subsequently gets carried from inlet to outlet section. The fluid is made to overcome the pressure prevailing at the outlet section and subsequently exit through it; therefore, compression is inherent in this process. To avoid wear and tear of parts, a small clearance is maintained in between the rotors and also between the lobe's tips and side walls. However, due to this clearance, some amount of fluid keeps flowing back from outlet section into the working chamber of pump due to the existing pressure gradient [2]. This flow of fluid is termed as leakage flow and the same must be minimized to maximise the efficiency of the machine [3].

The profile and shape of the lobes in a particular lobe pump determine the efficiency of the same. Many researchers have worked on examining the exact impact of profile shape on pump efficiency and tried to further optimise the same [4] [5] [6] [7]. Tong *et al.* [8] defined a new parameter named pumping ratio which is a function of rotor geometry. They stated that the flow rate through pumps could be enhanced further using the pumping ratio. Tong *et al.* [9], in their synthesis procedure, used a specific flow rate expression which is a function of lobe pitch and non-circularity to generate the optimum profile of rotor. Based on the pitch and deviation function of lobes, Yang *et al.* [10] derived a specific flow rate formula which is applicable for both circular and non-circular pitch curves. Yao *et al.* [11] presented a mathematical model and proposed a unique helical tooth profiled lobe pump. They argue that this specific design of tooth profile of lobes provides enhanced fluid flow rate and reduced peak pressure of pump. Even though many researchers have proposed improved design of lobes and rotor for lobe pump, it's the specific requirement of industry and few design constraints, which mostly determines the type and profile of lobes.

Because of the recent advances in computational methods and the inherent cost-effectiveness of simulation over experimentation, many researchers and designers are using computational fluid dynamics (CFD) simulation to validate their design of rotating machines. Moreover, other complex scenarios involving challenging physics such as transfer of proton in fuel cells and fluid-solid interaction in pressure vessels, are also simulated using CFD tools [12] [13]. Traditionally, simulation of rotating machines is performed with help of moving rotating frames (MRF) set up. Capurso *et al.* [14] used CFD simulations and MRF philosophy to propose a new impeller for centrifugal pumps with enhanced efficiency. Similarly, Valdes *et al.* [15] used MRF philosophy to study the performance of electrical submersible pumps handling non-Newtonian fluids. However, MRF is a steady state approximation of the rotating domains. The CFD solver typically creates a thin volumetric region of discretised cells (called mesh ele-

ments) around the rotating body, whereas the actual rotating body remains static throughout the simulation [16]. The MRF approach is suitable for rotating domains where the clearance between the rotating part and the stationary part is significant such as fans and turbines. However, in case of lobe pump the moving domain keeps changing its shape and size with gradual degree of lobes rotation. The clearance between the rotors and the surrounding wall varies from a fraction of a millimetre to a few hundreds of millimetres within one rotation of lobes. The discretised domain must adopt to the changing shape and size of the moving domain dynamically to capture the process accurately.

Though many researchers and designers have attempted to study the performance of lobe pump numerically, the constantly varying size of the moving domain and the transient nature of the pulsatile leakage flow makes the process a very challenging one. Furthermore, the unavailability of suitable algorithms to generate grids for this kind of applications limits the scope of using numerical techniques in this field [17]. Many researchers have even tried to benchmark the process of capturing the domain deformation with respect to the rotation of lobes. Therefore, an accurate algorithm which can replicate the lobes rotation in terms of dynamically changing grids (or mesh) and subsequent transport of fluid in transient state is equally important, as is the design of a new lobe pump. Rane *et al.* [18] used an algebraic grid generation algorithm to simulate a screw compressor with variable pitch between rotors. Kovacevic *et al.* [19] [20] used similar algebraic grid generation technique along with a boundary adoption method to simulate screw compressors. Kethidi *et al.* [21] performed CFD simulation to evaluate the effect of various turbulence models on velocity prediction inside screw compressors. Joshi *et al.* [22] studied the role of clearance on performance of lobe pump and proposed a static model for the same. Hsieh *et al.* [23] [24] used a CFD model named PumpLinx to study the differences between a cylindrical and screw type roots pumps. However, in all the studies reported above, either the simulation considered the discretised flow domain (or mesh) as static or an in-house CFD code is used which is proprietary in nature. Additionally, the capacity of the pump in all the studies are either small or is not exclusively mentioned.

Lobe pumps with high capacities are expected to have higher amount of leakage flow. In lobe pump operation, leakage flow has a strong bearing on the pressure pulsations inside chamber [25]. Additionally, leakage flow also contributes significantly to the unsteady flow field inside the chamber [26]. Lately, there has been a shift from bi-lobes to tri-lobes lobe pump because of the advantages in terms of reduced pressure pulsations and vibrations. However, carrying out performance simulation of lobe pump with high capacity is an extremely challenging task and to the best of the author's knowledge there has been no dynamic simulation of this capacity reported in literature earlier. In the present study, a unique combination of user-defined-functions (UDFs) and meshing strategies is employed to capture the rotation of the lobes of a newly designed

lobe pump and to dynamically adapt to the changing shape and size of the moving domain. The lobe pump under study is a tri-lobe industrial pump with capacity in the range of 18,000 - 20,000 Nm³/hr. In this study, commercially available CFD solver Ansys Fluent 18.1 has been used to simulate the lobe pump and to evaluate its performance. The pressure fluctuation inside the pump is predicted using the numerical model and the trends are validated with literature values. The power requirement at shaft, which is very crucial for a designer, is predicted by the present model. Elaborate discussion on the methodology is provided in section 2.0. The schematic of the lobe pump is depicted in **Figure 1**. The inlet and outlet section are extended significantly to eliminate the entry and exit effects in simulation.

2. Methodology

To accommodate the deforming boundary of the moving domain, Ansys Fluent provides options such as mesh smoothing and re-meshing. When the boundary displacement is still comparable to the local cell sizes (initial stage of rotation), the option of smoothing is invoked [16]. In the present simulation the spring based smoothing option is used which basically retains the total number of nodes while adjusting the mesh elements during rotation. When the boundary displacement becomes significantly large, the re-meshing function is invoked. The 2.5D re-meshing option is used in the present simulation which stipulates the surface mesh on top and bottom surfaces to be strictly triangular. Therefore,

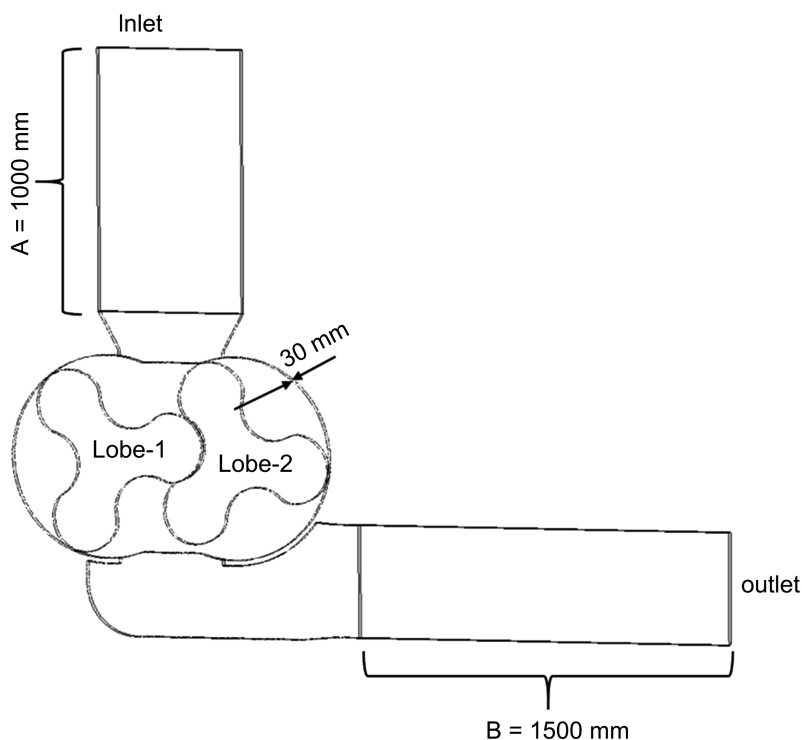


Figure 1. Schematic of lobe pump with extended inlet and outlet portions. “A” is the extended length at inlet and “B” at outlet.

only pyramidal mesh elements are generated in the moving domain. Considering the symmetry of the model along its thickness, only a thin strip of the model with 30 mm thickness is discretized for simulation. The variable clearance between the rotor and the surrounding wall makes the re-meshing process a challenging one. It is recommended to have uniform distribution of meshes along the periphery of the surrounding wall.

After generating a fixed set of mesh elements, the next task is to affect the mesh motion in CFD solver. In the present simulation, the motion of the lobes is guided by a set of two UDFs. These UDFs are developed on a programming language platform which passes on critical information such as the name of the rotating surface, the speed and direction of rotation to the solver. In transient simulations, the size of time step is critical to the accuracy of solution. In this simulation the time step size is carefully chosen by considering the smallest length scale (mesh element) and the anticipated velocity in the domain, which ensures that there is no compromise on accuracy at the same time there is no unnecessary delay in obtaining solution. The top and bottom surface of the pump are assigned as symmetric boundary conditions as those are the boundaries of chopped domain. In dynamic simulation setting, these surfaces are marked as deforming bodies, one with re-meshing option and the other without it. The transient simulation is performed as per the design conditions of the pump.

Variation of pressure and velocity values inside the blower, with respect to the rotation of lobes is predicted in the simulation. The predicted trend of pressure variation is compared with the same of Sun *et al.* [1] for validation of the numerical model. After successful validation, performance of the pump is predicted in terms of pressure contour and velocity vector plots. Finally, the power requirement at the shaft is estimated by using the predicted values. The simulation is a part of the overall design validation of the lobe pump for a specific industrial requirement.

3. Numerical Details

3.1. Computational Domain

The flow model for the pump is depicted in **Figure 2**. **Figure 2(a)** shows the actual flow model which has a thickness of more than 1 meter, **Figure 2(b)** shows the chopped domain of 30 mm thickness. The meshed flow domain is depicted in **Figure 3(a)**. Hexahedral mesh elements are generated on the inlet and outlet pipes and pyramidal mesh elements are generated on the moving domain. To extract CFD data and to compare the same with literature, five distinct points are created in the moving domain and the same is depicted in **Figure 3(b)**. Owing to the symmetric nature of the blower about the axis of rotation, only one rotor side of the blower is considered for data extraction and comparison. To eliminate entry effect and to avoid numerical instability, the inlet and outlet pipes are extended by a length of 1000 mm 1500 mm respectively.

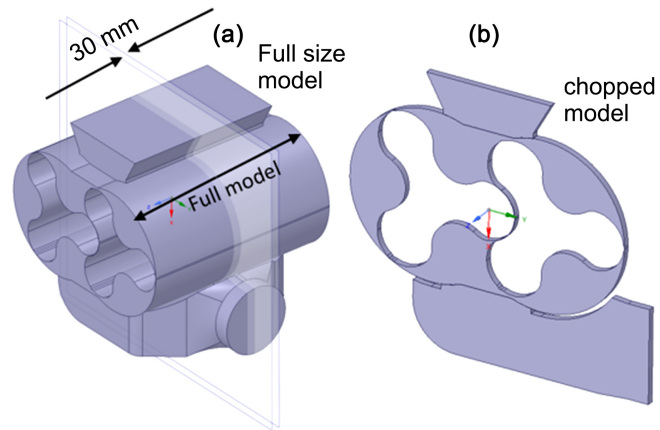


Figure 2. Flow model of lobe pump. (a) The whole model; (b) Chopped model with 30 mm strip.

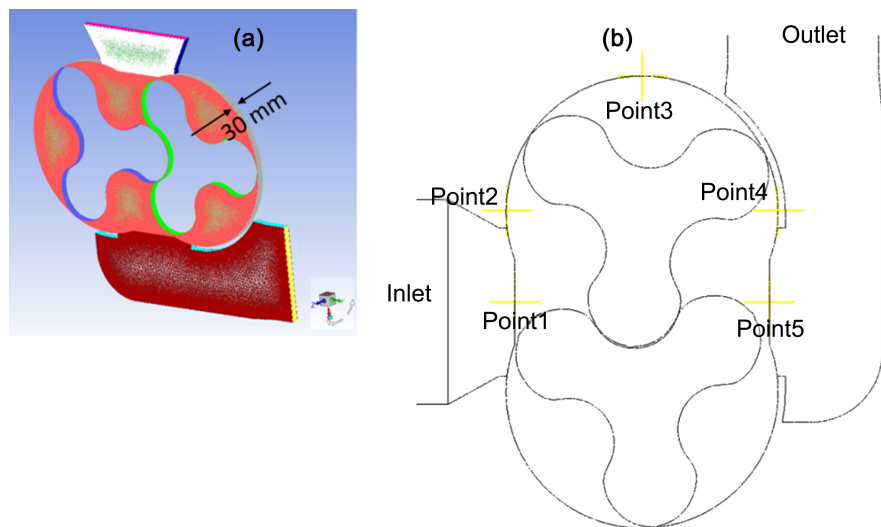


Figure 3. (a) Meshed flow domain of lobe pump and (b) Pressure prediction points created in simulation: Point 1 to point 5.

3.2. Solver Details

The present CFD solver is a finite-volume based commercial CFD solver. The governing equations are the conservation of mass, conservation of momentum (Navier-Stoke equations) and conservation of energy, as produced below.

$$\frac{\partial \rho}{\partial t} + \nabla \cdot (\rho \vec{v}) = S_m$$

$$\frac{\partial}{\partial t} (\rho \vec{v}) + \nabla \cdot (\rho \vec{v} \vec{v}) = -\nabla p + \nabla \cdot (\vec{\tau}) + \rho \vec{g} + \vec{F}$$

$$\frac{\partial}{\partial t} (\rho E) + \nabla \cdot (\vec{v} (\rho E + p)) = \nabla \cdot \left\{ k_{eff} \nabla T - \sum_i h_j \vec{J}_j + (\vec{\tau}_{eff} \cdot \vec{v}) \right\} + S_h$$

where,

S_m is the mass added to the continuous phase from discrete phase,

p is static pressure,

$\bar{\tau}$ is the stress tensor,
 \vec{F} is external body force,
 E is the total energy,
 k_{eff} is the effective thermal conductivity,
 \vec{J}_j is the diffusion flux of species j and
 S_h is the heat of chemical reaction.

A predictor-corrector algorithm namely SIMPLE, is used for pressure velocity coupling. For discretizing the pressure and diffusion terms, a second-order central differencing scheme is used and for the convective terms, a second-order upwind scheme is used. The standard k- ϵ turbulence model with standard wall functions has been chosen as the turbulence model for simulation. Air as ideal gas is considered as the working fluid. The convergence criteria for iterative calculations used in the CFD simulations are as follows. The minimum root-mean-square value of the residual for solving x , y , z velocity components and the turbulent equations is $1e-04$.

3.3. Boundary Conditions

The boundary conditions for simulation are prescribed as per the design parameters of the concerned lobe pump. The inlet is prescribed with a total pressure value of 93,000 Pa whereas the outlet is prescribed with a static pressure value of 190,000 Pa. The temperature of incoming air is maintained at 40°C. Both rotors are assigned a rotational speed of 740 RPM, one opposing the other. Turbulent intensity (the ratio of root-mean-square of the velocity fluctuations to the mean flow velocity) and hydraulic diameter are used to specify the turbulence parameters at the inlet and outlet of the domain. Ansys [16] recommends to use the following formula to have a gross estimation of the turbulent intensity for flow inside ducts,

$$I = \frac{U'}{U_{avg}} = 0.16 \left(\text{Re}_{D_H} \right)^{-\frac{1}{8}},$$

where I is the turbulence intensity, U' is the root-mean-square of the velocity fluctuations, U_{avg} is the mean flow velocity and Re_{D_H} is the Reynolds number of the flow based on hydraulic diameter. For a flow with a Reynolds number value of 50,000, the turbulent intensity value is close to 4% [16]. Therefore, for the present simulation the turbulent intensity is assigned as 5%.

4. Results and Discussion

4.1. Validation of Numerical Model

The numerical model used in the analysis of the lobe pump must be validated with either experimental values or literature. Since the concerned lobe pump is an industrial pump with higher capacity, experimental data of its performance is not openly available. In this regard, the pressure values reported by Sun *et al.* [1] for a smaller sized lobe pump are used as the basis for validation in the present

simulation. The pressure built-up by the pump in one complete rotation as predicted in present numerical simulation is compared with the same reported by Sun *et al.* [1] in **Figure 4**. As discussed by Sun *et al.* [1], the suction and displacement processes give rise to minimal pressure fluctuations as the fluid pocket is still in contact with the inlet chamber. The pressure fluctuation trend in this phase predicted by present simulation is in line with the same reported by Sun *et al.* [1]. Compression in lobe pump is an instantaneous process and the maximum pressure rise happens during this process. As depicted in **Figure 4**, the sudden rise in pressure due to compression of fluid is precisely captured in simulation. The trends of pressure rise in present simulation and literature are similar. The exhaust process witnesses significant pressure fluctuation because of the leakage of fluid back from outlet section. The same is manifested in **Figure 4**, both in case of literature and present simulation.

Sun *et al.* [1] measured the instantaneous pressure fluctuation at five distinct points inside the fluid chamber by placing pressure sensors at those points. All five points lie on one rotor side, considering the symmetrical nature of the blower. Similarly, in the present situation five numbers of points are created to extract CFD data and to compare with literature. The points created are demonstrated in **Figure 3(b)**. The predicted variation of instantaneous pressure at these points is compared with the same from literature in **Figures 5-8**.

Point 1 and point 2 are situated near the inlet section and they witness the process of suction and displacement. As demonstrated earlier in **Figure 4**, these two processes experience minimal pressure fluctuations. In **Figure 5** and **Figure 6**, both in case of literature and simulation, the pressure at these two points fluctuates about the value of inlet pressure with small amplitudes. Due to the proximity of point 3 to the compression region, the pressure sensor placed near point 3 starts receiving occasional spikes in pressure value. The same is depicted in **Figure 7(a)**. In the present simulation also, the occasional spikes in pressure

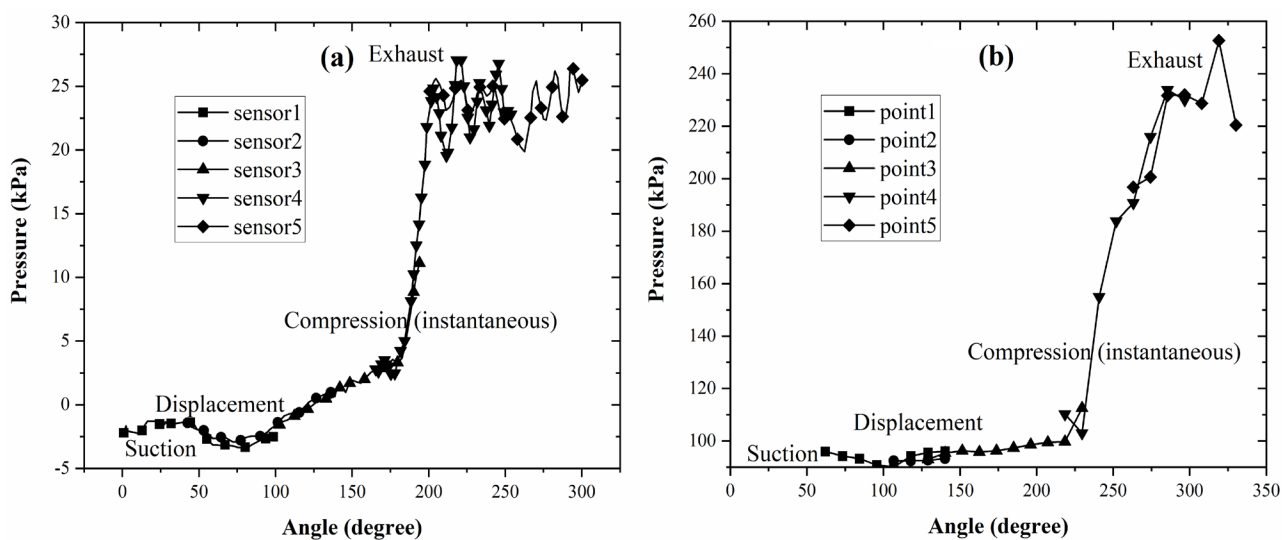


Figure 4. Pressure variation with respect to degree of lobes' rotation (a) literature (b) simulation.

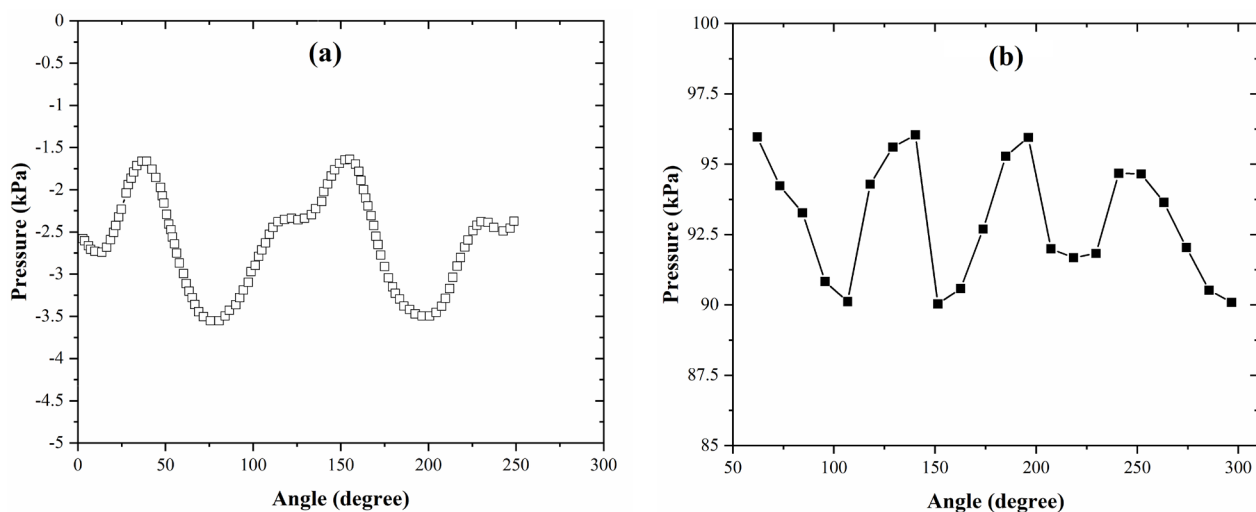


Figure 5. Pressure variation at point-1 (a) literature (b) simulation.

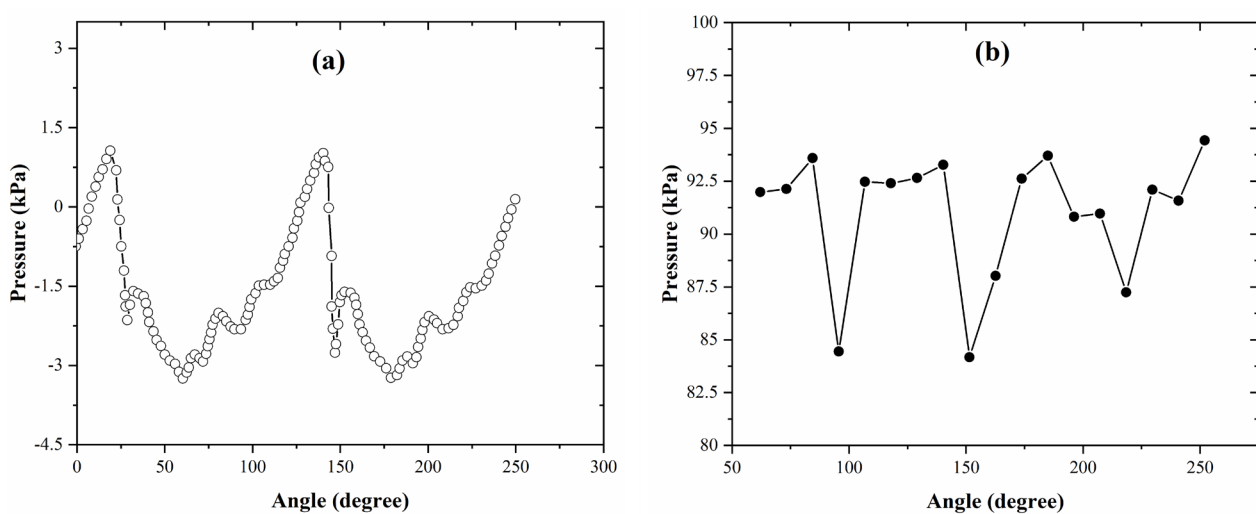


Figure 6. Pressure variation at point-2 (a) literature (b) simulation.

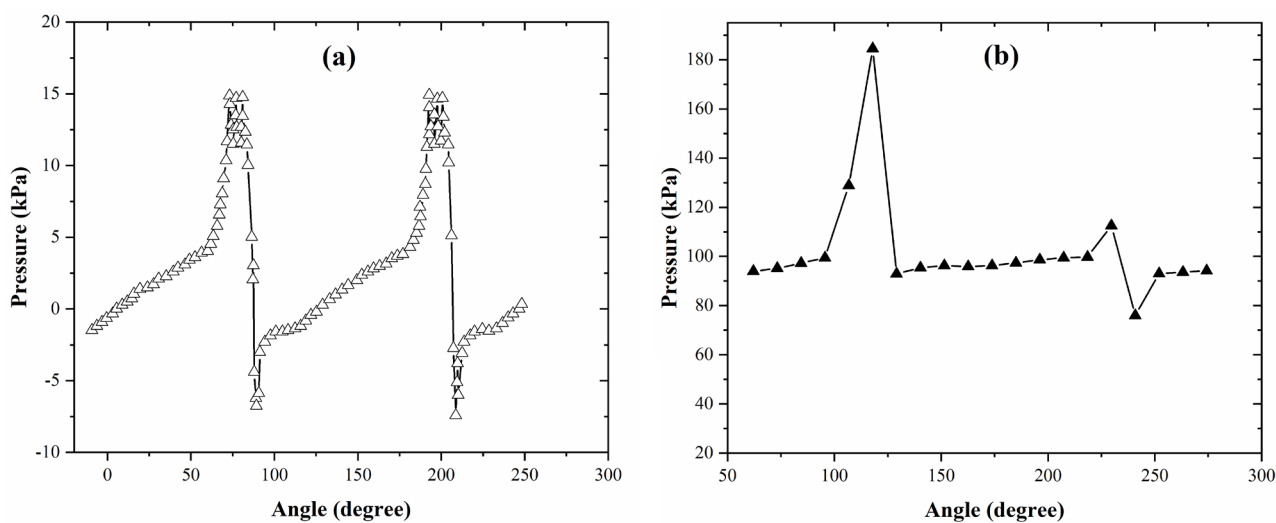


Figure 7. Pressure variation at point-3 (a) literature (b) simulation.

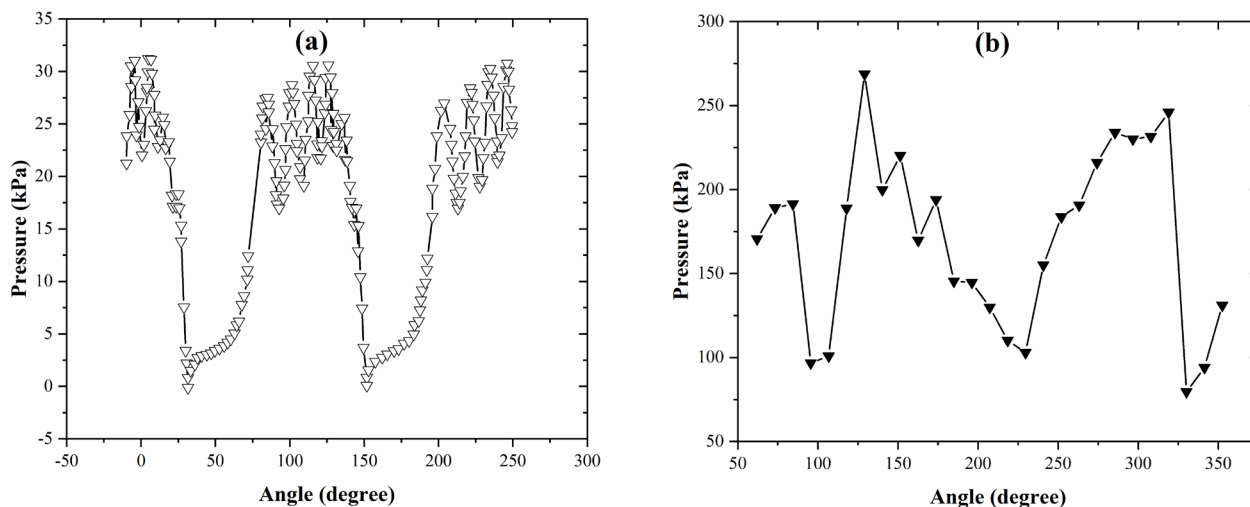


Figure 8. Pressure variation at point-4. (a) literature (b) simulation.

value can be noticed in **Figure 7(b)**. Point 4 falls under the region of compression, accordingly there is maximum pressure rise recorded by the sensor placed at point 4. The same is depicted in **Figure 8**, for both literature and present simulation. The sensor deployed near point 5 witnesses pressure fluctuation due to the leakage flow from outlet section. The pressure fluctuates about the outlet pressure value. In simulation also, the pressure extracted at point 5 fluctuates about the outlet pressure. However, in the literature case the oscillation in pressure value is more compared to the same in simulation case. The end portions of both the curves in **Figure 4(a)** and **Figure 4(b)** demonstrates this discrepancy. Sun *et al.* [1] concluded that the arrangement of outlet pipes is crucial in deciding the pressure fluctuation trend inside the chamber of lobe pump. They observed that the case with narrower outlet pipe matches more closely with experimental results. In the present simulation case, the inlet and outlet pipes are just continuation of the casing of lobe pump. The relatively fewer oscillations near point 5 in simulation case as observed in **Figure 4(b)**, could be attributed to this wider outlet pipe in comparison to literature case. It may be noted that at all the five points, the trends of pressure variation in case of literature and present simulation are same. The time cycle of pressure fluctuation also is similar in both the cases. This is a characteristic of the rotation of lobes inside the lobe pump; the same is captured accurately in present simulation and is validated with literature. Therefore, these plots along with the ones depicted in **Figure 4**, may be treated as the validation plots of the present simulation.

4.2. Pressure and Velocity Fields inside Lobe Pump

After successful validation of the numerical model, pressure and velocity fields inside the pump are predicted using CFD simulations. The variation of these parameters with respect to gradual degree of lobes rotation in a complete cycle is captured. Contour plots of pressure as predicted in the present simulation are reported in **Figure 9**. The pocket of air entrapped inside the working chamber

(denoted as WC in the plots) is traced along the degree of rotation. The pressure changes inside the WC are reported at five discrete degrees of rotations. As discussed in section 4.1, each value of degree of rotation reported here corresponds to a specific process out of the four processes discussed *i.e.* suction, displacement, compression and exhaust and the same can be correlated with **Figure 4**. **Figure 9** shows the pressure contour plots of air at a middle plane at the five different degrees of rotation. At 140° of rotation, the WC is still very close to the inlet section for which the pressure experienced by air inside WC is identical to the inlet pressure of 93 kPa. As discussed in section 4.1, the pressure variation during suction and displacement process is not significant. Therefore, the pressure experienced by the WC at 173° of rotation is also identical to the same at 140°, the first one corresponding to suction and the later corresponding to displacement processes. As depicted in **Figure 4**, compression in the present simulation starts only at around 240° of rotation. Therefore, at 218° of rotation also, the pressure inside the WC is still in the range of inlet pressure. At 230° of rotation, the effects of compression are just starting to show off and the pressure inside the WC is in the range of 110 - 115 kPa, which is marginally higher than the inlet pressure. At 252° of rotation, compression has already been in process and the same is manifested in **Figure 9**. The pressure in the WC is in the range of 185 kPa which indicates the process of compression is already in place.

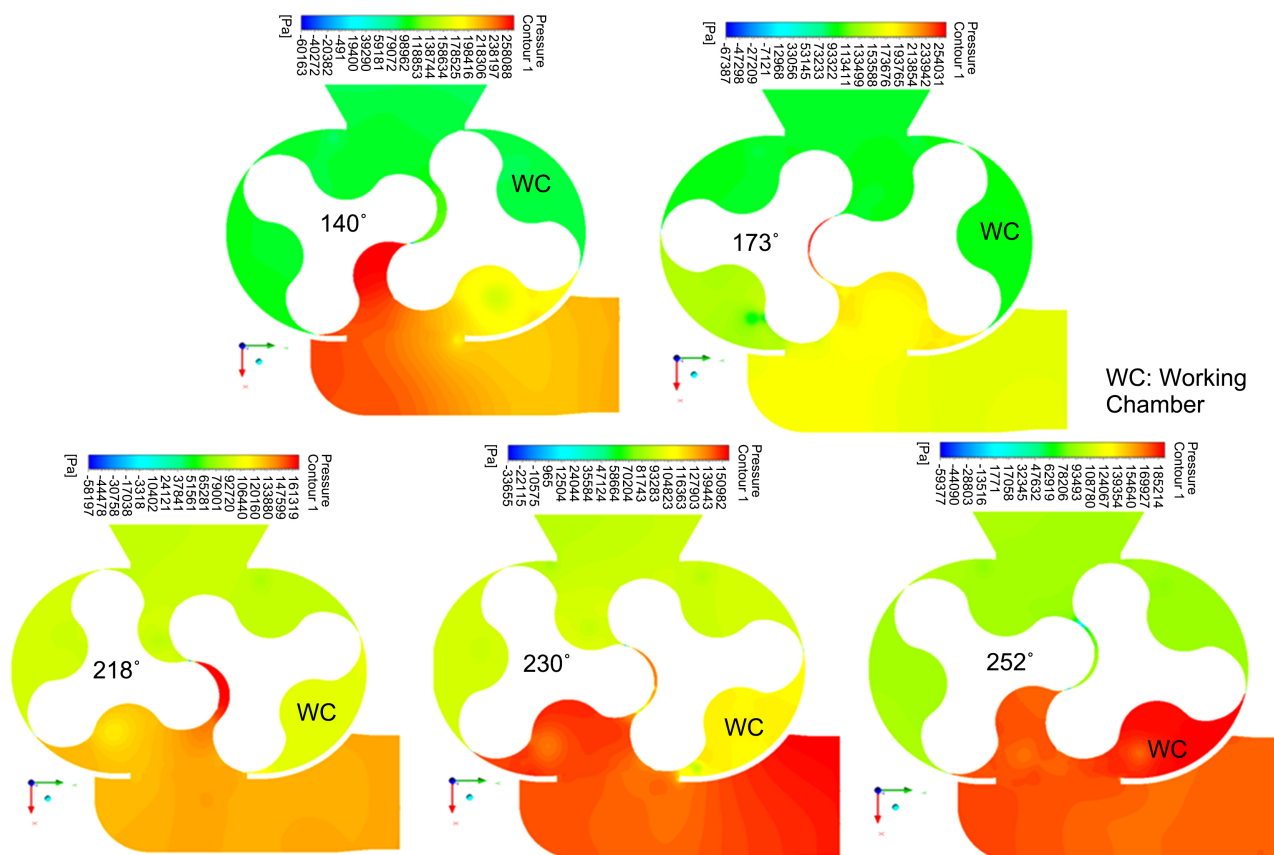


Figure 9. Pressure contour plots at different stages of lobe rotation. WC: Working Chamber.

Figure 10 depicts the velocity vector plots extracted on the same middle plane. The plots are extracted exactly at the same degrees of rotation as in case of **Figure 9** for pressure contour plots. Therefore, the movement of WC is also same in all the plots from **Figure 9** to **Figure 10**. From all the plots in **Figure 10**, it can be observed that the particular WC which is already approaching the outlet section, keeps receiving the leakage fluid which flows back into it. The same is depicted in terms of strong re-circulation and reverse velocity vectors in all the plots near outlet section. From the plots depicted in **Figure 9**, it is established that the pressure built-up in the lobe pump is both in line with literature values and also as per the design standards. From **Figure 10**, it is established that the leakage flow is consistently present during lobes rotation and the velocity values are in line with design standards. Therefore, the lobe pump is satisfactory from a designer's perspective.

4.3. Calculation of Power Requirement at Shaft

The power requirement at shaft for lobe pump, as given by [27] is calculated by the following formula

$$P = 0.00436 \times V_{ERV} \times N \times \Delta P + FHP$$

where,

P is the power requirement at shaft in BHP;

V_{REV} is the displacement (m^3) in one rotation;

N is the speed of rotation in RPM;

ΔP is the pressure rise (Pa);

FHP is the frictional horse power.

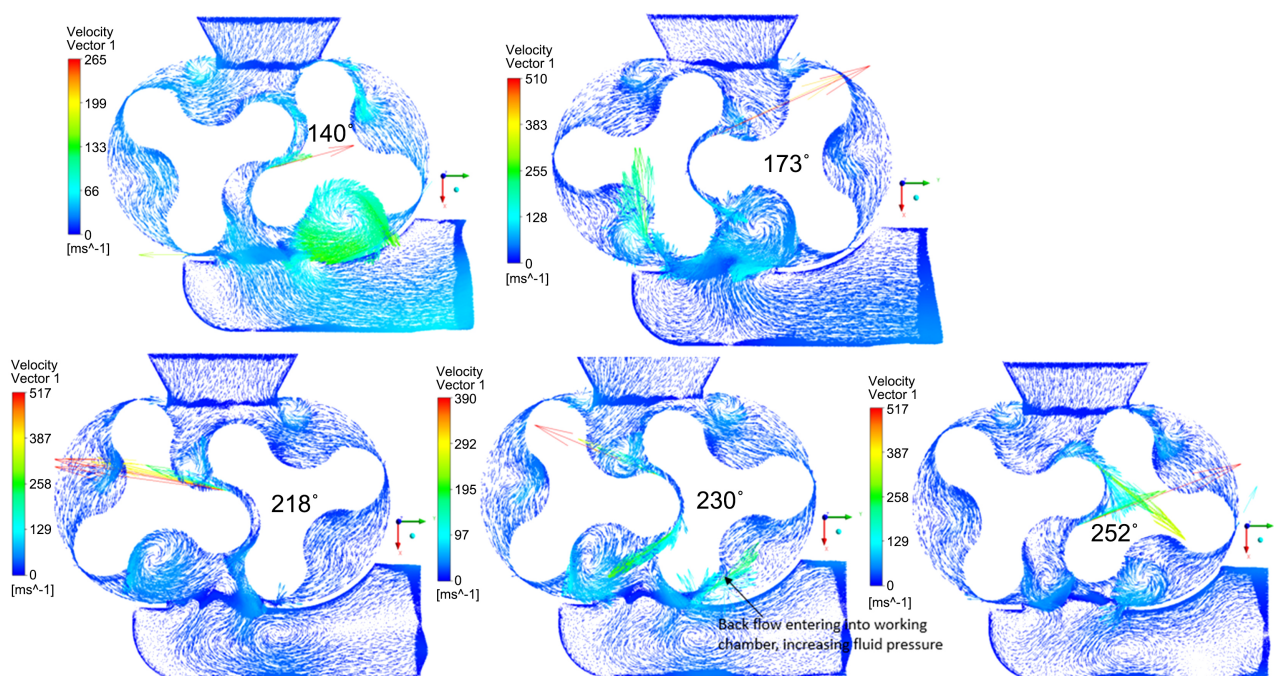


Figure 10. Velocity vector plots at different stages of lobe rotation.

Table 1. Comparison of power requirement at shaft between theoretical and CFD predicted value.

Parameters	Theoretical	Predicted
N (RPM)	745	745
VREV (m ³)	0.44169	0.01257
Pinlet (Pa)	93,400	93,187
Poutlet (Pa)	187,000	187,000
ΔP (Pa)	93,600	93,813
P (BHP)	2238 W + FHP = 3 BHP + FHP	$(1265/30) \times 63.83 \text{ W} + \text{FHP} = 2691 \text{ W} + \text{FHP} = 3.61 \text{ BHP} + \text{FHP}$

To obtain V_{REV} of CFD simulation, the average flow rate predicted for one cycle of rotation is used. Using the above formula, the required power at shaft is calculated. The comparison of power requirement between theoretical value and CFD predicted value is depicted in **Table 1**. Since the comparison is for the power required at shaft solely due to displacement of air, the frictional horse power is not calculated in both the cases.

As depicted in **Table 1**, the theoretical power requirement at shaft is 3 BHP + FHP, whereas the same predicted by CFD analysis is 3.61 kW + FHP. It is to be noted that CFD analysis is carried out for a thin strip which extends 15 mm in both directions from centre line. The power requirement for this thin strip is calculated as 63.83 W + FHP. To estimate the power requirement for the whole pump, a factor of 42.167, which when multiplied with model thickness gives rise to total thickness of pump, is multiplied with this power. This leads to the assumption that the blower is entirely symmetric in direction of its thickness. In reality, the inlet and outlet pipes do not extent till the extreme edges of the blower, rather those are significantly narrower. The marginally higher estimation of power requirement for whole pump in case of CFD simulation can be attributed to this factor. It is to be noted that the predicted value of power requirement at shaft is reasonably accurate in industrial standard and this way of calculating power requirement may be relied by designers of lobe pump.

5. Conclusions

The performance of a newly designed tri-lobe industrial lobe pump of high capacity is simulated by using commercial CFD solver Ansys Fluent. A unique combination of UDFs and meshing strategies is employed to capture the rotation of the lobes and to dynamically adapt to the changing shape and size of the moving domain. The numerical method is validated by comparing the simulated results with the results of Sun *et al.* [1]. The variation in pressure values for a complete rotation, as predicted by CFD simulation is mostly in line with litera-

ture. The processes of suction, displacement, compression and exhaust are accurately captured in the simulation and the pressure fluctuation during exhaust process is also compared with literature values. Five virtual points are created inside the flow domain which replicates the five pressure sensors used in literature. The pressure fluctuations at these points, as captured by simulation are similar to the ones reported in literature. Point 1 and Point 2 correspond to the process of suction and discharge, accordingly there is minimal pressure fluctuation reported at these points. Due to the proximity of Point 3 to compression region, there are occasional spikes in pressure value reported at Point 3. Point 4 falls under the compression region, accordingly the maximum pressure rise is reported at this point. All the reported pressure fluctuation trends are in line with the same reported in literature.

Further, pressure and velocity values of air for different degrees of lobes rotation are predicted and contour and vector plots are extracted. The movement of a specific WC is traced along the degree of rotation of lobes. At five discrete degrees of rotation, the pressure contour and velocity vector plots are reported. Up to 218° of rotation, the position of WC corresponds to the process of suction and displacement. Therefore, the pressure witnessed by WC at these degrees is in the range of inlet pressure of 93 kPa. At 230° of rotation, the WC is just about to enter the compression zone. The effect of compression is starting to show off here and the pressure is in the range of 110 - 115 kPa. At 252° the compression is already in process and the WC witnesses pressure values around 185 kPa *i.e.* in the range outlet pressure. Each pressure value inside the WC conforms to the particular process in which the working chamber is operating. To examine the presence of leakage flow, velocity vector plots are extracted at the same five discrete degrees of rotation. These plots show that the particular WC which is already approaching the outlet section, keeps receiving the leakage fluid which flows back into it. The same is depicted in terms of strong re-circulation and reverse velocity vectors in all the plots near outlet section. Finally, the power requirement at the shaft of rotation is estimated from the simulated values. The estimated value of power requirement is 3.61 BHP + FHP whereas the same calculated theoretically is 3 BHP + FHP. The discrepancy is attributed to the assumption of symmetry of pump along the thickness. Transient simulation using this unique strategy serves the purpose of validating the design of tri-lobe industrial lobe pump of high capacity, which is the need in pumps industry.

Funding

This research did not receive any specific grant from funding agencies in the public, commercial, or not-for-profit sectors.

Conflicts of Interest

The authors declare no conflicts of interest regarding the publication of this paper.

References

- [1] Sun, S., Zhao, B. and Peng, X. (2017) Three-Dimensional Numerical Simulation and Experimental Validation of Flows in Working Chambers and Inlet/Outlet Pockets of Roots Pump. *Vacuum*, **137**, 195-204. <https://doi.org/10.1016/j.vacuum.2017.01.005>
- [2] Burmistrov, A., Belyaev, L., Ossipov, P., Fomina, R. and Khannanov, R. (2001) Combined Experimental and Calculation Study of Conductance of Lobe Pump Channels. *Vacuum*, **62**, 331-335. [https://doi.org/10.1016/S0042-207X\(01\)00284-6](https://doi.org/10.1016/S0042-207X(01)00284-6)
- [3] Valdes, L.C., Barthod, B. and Perron, Y.L. (1999) Accurate Prediction of Internal Leaks in Stationary Dry Roots Vacuum Blowers. *Vacuum*, **52**, 451-459. [https://doi.org/10.1016/S0042-207X\(98\)00330-3](https://doi.org/10.1016/S0042-207X(98)00330-3)
- [4] Wang, P.Y., Fong, Z.H. and Fang, H.S. (2002) Design Constraints of Five-Arc Roots Vacuum Pumps. *Proceedings of the Institution of Mechanical Engineers Part C*, **216**, 225-234. <https://doi.org/10.1243/0954406021525151>
- [5] Hseih, C.F. (2015) A New Curve for Application to the Rotor Profile of Rotary Lobe Pumps. *Mechanism and Machine Theory*, **87**, 70-81. <https://doi.org/10.1016/j.mechmachtheory.2014.12.018>
- [6] Hwang, Y.W. and Hseih, C.F. (2006) Study on High Volumetric Efficiency of Roots Rotor Profile with Variable Trochoid Ratio. *Proceedings of the Institution of Mechanical Engineers Part C*, **220**, 1375-1384. <https://doi.org/10.1243/09544062JMES176>
- [7] Hseih, C.F. and Hwang, Y.W. (2007) Study on High-Sealing of Roots Rotor with Variable Trochoid Ratio. *Journal of Mechanical Design*, **129**, 1278-1284. <https://doi.org/10.1115/1.2779897>
- [8] Tong, S.H. and Yang, D.C.H. (2000) On the Generation of New Lobe Pumps for Higher Pumping Flowrate. *Mechanism and Machine Theory*, **35**, 997-1012. [https://doi.org/10.1016/S0094-114X\(99\)00048-8](https://doi.org/10.1016/S0094-114X(99)00048-8)
- [9] Tong, S.H. and Yang, D.C.H. (2000) Rotor Profile Synthesis for Lobe Pumps with Given Flowrate Functions. *Journal of Mechanical Design*, **127**, 287-294. <https://doi.org/10.1115/1.1798271>
- [10] Yang, D.C.H. and Tong, S.H. (2002) The Specific Flowrate of Deviation Function Based Lobe Pumps-Derivation and Analysis. *Mechanism and Machine Theory*, **37**, 1025-1042. [https://doi.org/10.1016/S0094-114X\(02\)00065-4](https://doi.org/10.1016/S0094-114X(02)00065-4)
- [11] Yao, L., Ye, Z. and Dai, J.S. (2005) Geometric Analysis and Tooth Profiling of a Tri-Lobe Helical Rotor of Lobe Pump. *Journal of Materials Processing Technology*, **170**, 259-267. <https://doi.org/10.1016/j.jmatprotec.2005.05.020>
- [12] Louis, K. (2024) Simulation and Analysis of the Effects of Pressure and Temperature on the Output Voltage of Proton Exchange Membrane Fuel Cells. *Journal of Power and Energy Engineering*, **12**, 1-16. <https://doi.org/10.4236/jpee.2024.122001>
- [13] Uddin, M. and Yousuf, M. (2022) Numerical Simulation of CFD and Fluid-Structure-Interaction (FSI) of Steady Flow in a Stenotic Vessel. *Open Journal of Modelling and Simulation*, **10**, 255-266. <https://doi.org/10.4236/ojmsi.2022.103013>
- [14] Capurso, T., Bergamini, L. and Torresi, M. (2019) Design and CFD Performance Analysis of a Novel Impeller for Double Suction Centrifugal Pumps. *Nuclear Engineering and Design*, **341**, 155-166. <https://doi.org/10.1016/j.nucengdes.2018.11.002>
- [15] Valdes, J.P., Becerra, D., Roza, D., Cediell, A., Torres, F. and Asuaje, M. (2020) Comparative Analysis of an Electrical Submersible Pump's Performance Handling Viscous Newtonian and Non-Newtonian Fluids through Experimental and CFD Ap-

- proaches. *Journal of Petroleum Science and Engineering*, **187**, Article ID: 106749. <https://doi.org/10.1016/j.petrol.2019.106749>
- [16] ANSYS. *ANSYS Fluent Theory and User's Guide*. ANSYS.
- [17] Bianchi, G., Rane, S., Kovacevic, A. and Cipollone, R. (2017) Deforming Grid Generation for Numerical Simulations of Fluid Dynamics in Sliding Vane Rotary Machines. *Advances in Engineering Software*, **112**, 180-191. <https://doi.org/10.1016/j.advengsoft.2017.05.010>
- [18] Rane, S., Kovacevic, A., Stosic, N. and Kethidi, M. (2013) CFD Grid Generation and Analysis of Screw Compressor with Variable Geometry Rotors. Centre for Positive Displacement Compressor Technology, SEMS City University, London. <https://doi.org/10.1533/9781782421702.11.601>
- [19] Kovacevic, A. and Smith, I.K. (2002) The Influence of Rotor Deflection upon Screw Compressor Performance. *VDI Berichte*, **1715**, 17-28.
- [20] Kovacevic, A., Stosic, N. and Smith, I.K. (2007) *Screw Compressors-Three Dimensional Computational Fluid Dynamics and Solid Fluid Interaction*. Springer-Verlag, Berlin.
- [21] Kethidi, M., Kovacevic, A., Stosic, N. and Smith, I.K. (2011) Evaluation of Various Turbulence Models in Predicting Screw Compressor Flow Processes by CFD. *7th International Conference on Compressors and Their Systems*, London, 5-6 September 2011, 347-357. <https://doi.org/10.1533/9780857095350.8.347>
- [22] Joshi, A.M., Blekhman, D.I. and Fleske, J.D. (2006) Clearance Analysis and Leakage Flow CFD Model of a Two-Lobe Multi-Recompression Heater. *International Journal of Rotating Machinery*, **2006**, Article ID: 079084. <https://doi.org/10.1155/IJRM/2006/79084>
- [23] Hseih, C.F. and Deng, Y.C. (2015) A Design Method for Improving the Flow Characteristic of a Multistage Roots Pump. *Vacuum*, **121**, 217-222. <https://doi.org/10.1016/j.vacuum.2015.09.001>
- [24] Hseih, C.F. and Zhou, Q.J. (2015) Fluid Analysis of Cylindrical and Screw Type Roots Vacuum Pumps. *Vacuum*, **121**, 274-282. <https://doi.org/10.1016/j.vacuum.2015.04.037>
- [25] Sun, S.K., Jia, X.H., Xing, L.F. and Peng, X.Y. (2018) Numerical Study and Experimental Validation of a Lobe Pump with Backflow Design. *Engineering Applications of Computational Fluid Mechanics*, **12**, 282-292. <https://doi.org/10.1080/19942060.2017.1419148>
- [26] Singh, G., Sun, S., Kovacevic, A., Li, Q. and Bruecker, C. (2019) Transient Flow Analysis in a Lobe Pump: Experimental and Numerical Investigations. *Mechanical Systems and Signal Processing*, **134**, Article ID: 106305. <https://doi.org/10.1016/j.ymsp.2019.106305>
- [27] https://www.pdblowers.com/wp-content/uploads/2016/11/rotary_positive_displacement_blower_calculations_1.pdf

Nomenclature

CFD	Computational Fluid Dynamics
MDM	Moving Dynamic Mesh
SIMPLE	Semi-Implicit Method for Pressure Linked Equations
A	Extended length of inlet section
B	Extended length of outlet section
k	Turbulent kinetic energy
ε	Turbulent dissipation rate
UDF	User Defined Functions
RPM	Rotations per Minute
I	Turbulent intensity
Re_{DH}	Reynolds's number of flow based on hydraulic diameter
WC	Working Chamber
P	Power requirement at shaft
V_{REV}	Displacement in one rotation
P_{inlet}	Pressure at inlet
P_{outlet}	Pressure at outlet
N	Speed of rotation
ΔP	Pressure rise
FHP	Frictional Head Loss